POLITECNICO DI TORINO
Repository ISTITUZIONALE

Capacitor charging method for I–V curve tracer and MPPT in photovoltaic systems

(Article begins on next page)

01 September 2025

Capacitor Charging Method for I-V Curve Tracer and MPPT in Photovoltaic Systems

Filippo Spertino[1], Jawad Ahmad[1], Alessandro Ciocia[1], Paolo Di Leo[1], Ali F. Murtaza[2], Marcello Chiaberge[3]

[1] Politecnico di Torino, Energy Department, [2] Department of Mechanical and Aerospace Engineering, [3] Department of Electronics and Telecommunication Engineering, corso Duca degli Abruzzi, 24 – 10129 Torino, Italy

Corresponding author:

Filippo Spertino

Politecnico di Torino, Energy Department

corso Duca degli Abruzzi 24, I-10129 Torino, Italy

e-mail filippo.spertino@polito.it

Abstract: The capacitor charging method can be used in Photovoltaic (PV) systems for two typical applications: a very simple and cheap way (1) to trace the *I-V* curve of a PV generator of whatever size and (2) to track the Maximum Power Point (*MPP*), especially when the partial shading occurs. The problem is the correct sizing of the capacitor in order to achieve accurate, uniform and smooth results. In the first application a simplified calculation to design quickly the capacitor is carried out. This is done only as a function of the main characteristics of the PV array and the most important datasheet parameters of the PV modules. In the second application a *MPPT* (*MPP Tracker*) circuit based on capacitor charging is designed and simulated in partial shading conditions. In these conditions the Power-Voltage (*P-V*) curve of a PV array is characterized by the presence of multiple maxima. The PV array is isolated from the load for a negligibly short period and is connected to an external capacitor. During the charging time, the proposed circuit tracks the global *MPP*. This circuit is easy to implement and shortens the duration needed for scanning the *P-V* curve of the array.

1.   Introduction

Solar energy is one of the most important renewable sources: it is clean, inexhaustible and free. PV power generation exhibits relatively high installation cost [1] and limited efficiency of solar cells. Photovoltaic (PV) arrays are used to directly convert solar into electrical energy. PV arrays are built by connecting many modules in series to form a string, by connecting strings in parallel to form an array, to obtain the desired levels of output voltage, current and power.

The monitoring of its performance during the operation is achievable by the measurement of current-voltage characteristic (*I-V*) of the array at the actual solar irradiance and ambient temperature. The Standard [2] is a reference in this topic: it describes "the minimum commissioning tests, inspection criteria and documentation expected to verify the correct operation of the system". At this aim, the typical size limits, i.e., ≤100 kWp as written in [3], of the commercial instrumentations (based on electronic loads) can be avoided with the adoption of the capacitor charging method as a curve tracer. Moreover, the curve tracer based on capacitive loads is simpler, cheaper and scalable from module level to array level. Nevertheless, it is required a detailed sizing of the capacitive load to optimize the duration and the accuracy of the measurements.

Then, the optimal extraction of power from PV arrays is quite challenging, as the power-voltage (*P-V*) characteristic of the arrays is highly non-linear and changes continuously with irradiance/cell temperature and shading conditions. Considering these issues, it is very important to operate a PV array at a point where maximum power could be obtained. *MPPTs* are used for this purpose. A variety of *MPPT* techniques have been reported in literature [4-7]. These methods vary in their accuracy, cost of implementation, types of sensors required, ability to operate properly in shading conditions and complexity of circuit. Conventional *MPPT* techniques are able to operate under uniform irradiance conditions. Fig.1 shows the *P-V* curve of a solar array under uniform irradiance conditions which exhibits only one peak. The tracking of such a *MPP* is not quite challenging for

conventional *MPPT* algorithms like Perturb and Observe (*P&O*). This is a simple technique and is adopted quite frequently for the PV systems in which all the modules in an array receive uniform solar irradiance.

However, in some cases the array may not be under uniform irradiance and may suffer from partial shading due to a variety of factors like shadows of nearby buildings, trees, and dirt, etc.. The problem of partial shading is almost inevitable under practical conditions. Out of 1000 building integrated PV systems installed in Germany, 41% suffered from partial shading [5]. Since the short circuit current of a solar cell is proportional to the irradiance, partial shading results in reduction of generated current from the shaded module. At the same time, the un-shaded modules continue to generate a high current. As the string current must be equal through all the series connected modules, the consequence is that the shaded module operates in the reverse bias region to conduct the larger current of the un-shaded modules. The shaded module consumes power due to reverse voltage polarity which results in the reduction of extractable power from the array. Also, the dissipation of power in shaded modules may lead to local overheating and hot spot problems. When the hot spots exceed the maximum power that can be sustained by PV cells, it will cause irreversible damage. To mitigate this problem, bypass diodes are connected across the terminals of groups of cells in each module of the string. This protection allows the array current to flow in the correct direction, even if some of the modules (or groups of cells) are completely shaded. However, another problem arises in electrical characteristic of PV array when bypass diodes are used. Because of the action of these diodes, multiple peaks appear in the *P-V* curve of a solar array during shading as shown in Fig. 2. For conventional MPPT techniques like *P&O*, all the maxima shown in Fig. 2 satisfy the condition of *MPP*. If the operating point tracked by the conventional technique is a *Local Peak* (*LP*), the output power from the array is significantly reduced. It has been reported in literature that the power loss due to the tracking of a *LP* could be as high as 70% [8]. Hence, conventional *MPPT* techniques do not operate properly under partial shading conditions.

In recent years, many studies have been performed on reducing the losses in PV systems due to partial shading. As a result of these studies, many *MPPT* techniques have been proposed for non-uniform irradiance conditions [3]. These techniques are broadly classified as hardware-based and software-based techniques. Hardware-based techniques include module-integrated DC-DC converters, multilevel converters, parallel-connected *MPPTs*, and power electronic equalizers, etc. [9]. Software-based techniques include Fibonacci search algorithm, artificial neural network based, Fuzzy logic based, and particle swarm optimization based *MPPTs*, etc. [10],[11]. Hardware-based *MPPTs* have the disadvantage of decreased reliability and efficiency, and increased system complexity and implementation cost. Software-based techniques usually exhibit algorithmic complexity and may require powerful microcontrollers, which naturally result in increased system cost [11]. For tracking the Global Maximum Power Point (*GMPP*) during partial shading, a periodic scan sequence of the *P-V* curve is frequently employed [5]. Due to the extended time required for the completion of this process, the production of energy from the array is reduced. Based on comprehensive study of the *P-V* characteristics of partially shaded arrays, [12] has proposed a technique which is capable of tracking the Global Peak (*GP*) of a PV array under non uniform irradiance conditions. Even though the *MPPT* technique does not require scanning the entire *P-V* curve, [13] has shown that the time required to perform such a scanning can be as high as 8.6 s. The *MPPT* algorithm proposed in [13] takes a long time ($\approx$1.1 s) to track *GP*. During the *GP* tracking the PV array is not operated at *MPP* which causes a considerable power loss.

The current paper proposes a *MPPT* method that identifies *GMPP* of a PV array under partial shading conditions. In this method the *P-V* curve of the array is scanned in a very short time, $\approx$5 ms. During the scanning process, the PV array is isolated from load and is connected to a completely discharged capacitor. Voltage of the array corresponding to *MPP* is measured and is kept in a droopless sample and hold (S&H) circuit for the operation of the *MPPT* circuit. The proposed circuit does not require complex computation and is easy to implement. The circuit is able to

operate successfully under uniform as well as partial shading condition. The proposed technique is suited for stand alone and grid connected PV systems in which the output of the DC-DC converter is connected to a storage device. The storage devices, as e.g. batteries and supercapacitors (*SC)* or ultracapacitors, store energy from the PV system and then deliver it to the local loads or grid [14]. In these systems, momentary isolation of the PV array from load for scanning purposes has a negligible effect on power quality issues.

This paper is organized as follows: Section II shows how the use of capacitors of different sizes affect the measurements carried out on PV generators. Section III derives simple formulas that link the measurement time to the size of the capacitor used for scanning the *I-V/P-V* curves of the PV generator. Section IV discusses the proposed MPPT circuit on the basis of formulas derived in Section III. In Section V the simulation results are given.

2.   The transient charging of a capacitor supplied by a PV generator

In the last years researchers [15] carried out measurements of *I-V* curves of whatever size PV arrays using different capacitive loads. The tests were useful to determine the parameters of the PV generators in conditions of natural light ($G\neq1000$ W/m^2) and cell temperature ($T\neq25°$C). The processed data were corrected at *STC* ($G_{STC} = 1000$ W/m^2, $T_{STC} =25$ °C) conditions and compared with the specifications from the manufacturers.

As well-known, the transient evolution of capacitor charging depends on the parameters of both the source (the PV generator) and the reactive load. Fig. 3 shows the classical single-exponential model of a solar cell [16] which supplies a capacitor modeled as the parallel of the capacitance (*C*) and the isolation resistance (R_C). An output current equation of the solar cell can be written as:

$$I(V) = I_{ph} - I_0 \cdot \left(\exp\left(\frac{V + I \cdot R_s}{m \cdot \frac{k \cdot T}{q}} \right) - 1 \right) - \left(\frac{V + I \cdot R_s}{R_{sh}} \right) \tag{1}$$

- photo-induced current I_{ph} (A) depending on material, irradiance and temperature;

- saturation current I_0 (A) of the semiconductor junction;

- physical quantities, i.e., the electron charge q (C) and the Boltzmann constant k (J/K);

- cell temperature T (K);

- quality factor m of the junction;

- series resistance R_s (Ω) and shunt (or parallel) resistance R_{sh} (Ω).

In this scheme the parasitic parameters of the solar cell are neglected. Nevertheless, when a PV generator is made of the parallel connection of strings and the strings are made of the series connection of PV modules (normally, a group of cells in series), the parasitic capacitance (junction and ground coupling) and leakage inductance are required [16] to understand the behaviour of the measuring circuit in Fig. 3.

In particular, during the tests, the transient charging starts from the open circuit condition for the PV generator and occurs at the closing of the power breaker (*PB*): after the step variation in the current signal, some oscillations appear (Fig. 4). These swings exhibit amplitudes and frequency depending on the external capacitance, as found in a second-order transient of a *RLC* circuit. As well-known, an increase of external capacitance implies a reduction of both amplitude and frequency. The points useful for tracing the *I-V* curve are taken after the initial oscillations in such a way as to correctly measure the short circuit current I_{sc}. If the extinction of the swings occurs when the voltage signal is still close to zero ($v(t) < 0.1V_{oc}$), it is possible to extrapolate, by linear regression in the *I-V* plane, the value of I_{sc}. For example, Fig. 4 shows the evolutions during the charging of different capacitors connected to a 235-Wp conventional poly-crystalline (p-Si) module. It can be noted that from the experimental tests, plotting the current signal as a function of the voltage signal, the maximum power P_{mpp}, with a measurement uncertainty of ±1%, does not change (Table I), when the capacitance is within 40—20,000 µF and the corresponding transient duration ranges from 0.5 to 211 ms.

On the other hand, if an unconventional (high-efficiency) technology is considered, i.e., the all back side contact (*BSC*) solar cell, the external capacitance must be higher to have an accurate *I-V* curve.

Table II shows the main parameters at *STC*, calculated by the prescriptions of [17] from the data measured at the test conditions shown in Fig. 5, where the closing of *PB* in Fig. 3 occurs at different instants to simplify the understanding of the transient evolutions. The *BSC* cells exhibit a higher leakage inductance and lower parasitic capacitance with respect to the conventional silicon technologies. As a consequence, the nearly constant current in the transient is settled at a value lower than the static photovoltaic current I_{ph} when the external capacitance is too low. Only the test carried out with the capacitance of 10 mF permits to obtain a correct dynamic *I-V* curve, which can be superimposed on the static curve obtainable with a variable resistive load. As a result, the parameters of the PV generator with the smallest capacitance are not correct: in the present case, P_{mpp} (*STC*) drops from 56 to 46 W, with a relative error $\approx 17\%$. It is remarkable to point out that the BSC solar cells cover a very limited share ($< 5\%$) of the market.

Then, if the experimental study is extended to the level of PV array, the capacitance accounting for the ground coupling is remarkable, because it increases with the number of PV modules connected each other. The consequence is the increment of the damping coefficient in the *RLC* transient evolution with a negligible impact of the swings. Therefore, the minimum value of capacitance to have a correct dynamic *I-V* curve is confirmed within some tens of microfarad.

3. Simplified calculation of transient capacitor charging

The current-voltage relationship is nonlinear and thus the solution of this equation requires an iterative method and noticeable computational burden, in particular in those applications in which the calculation of the *I-V* curve must be performed with high frequency and accuracy.

By adopting a piecewise approximation of the *I-V* curve, the diode behaviour in Fig. 3 is like an open circuit, when the operating points are in the portion from short circuit to maximum power conditions. In details, PV generators made of crystalline silicon exhibit a current at maximum power nearly equal to the short-circuit current ($I_{mpp} \approx 0.9$—$0.95 \cdot I_{sc}$). Thus, the PV generator can be considered a current source from short circuit to near maximum power condition, neglecting also the current leakage in

the shunt resistance. Moreover, from maximum power to open circuit conditions, the diode behaviour together with the series resistance R_s is like as a Thévenin equivalent. In this new simple model, the capacitance C is the only load connected to the generator, whereas the internal resistance R_C of the capacitor is assumed infinite.

I- First part: transient charging at constant current

An ideal current source supplies a resistance in series with a capacitor after the closing of the power breaker (Fig. 6.a). The current injection is provided by the parallel connection of N_p strings: every string gives $I_{ph} \approx I_{sc}$, which is the short circuit current of the N_c cells in series for each module inside the string.

$$i(t) = I_{sc} \cdot N_p \qquad \text{for} \quad 0 < t < t_0 \qquad (2)$$

At the beginning of the transient, the capacitor behaves as a short circuit with zero volts. The voltage increases linearly until the end of this part of the transient. The signal $v(t)$ is inversely proportional to the capacitance connected to the circuit and directly proportional to solar irradiance according to:

$$v(t) = \frac{1}{C} \int_0^{t_0} I_{sc} \cdot N_p \cdot dt = \frac{I_{sc} \cdot N_p}{C} \cdot t \qquad \text{for} \quad 0 < t < t_0 \qquad (3)$$

This transient expires at t_0, when the capacitor is charged at V_0: the meaning of the pair (t_0, V_0) is defined in the following subsection.

II- Second part: transient charging supplied by a voltage source

The successive portion of the transient begins at instant t_0. In this case (Fig. 6.b) an ideal voltage source $N_s V_{oc}$ supplies the resistor R_{eq} in series with the capacitor already charged at V_0. The forcing term $N_s V_{oc}$ represents the open circuit voltage of N_s series connected modules (made of N_c cells in series) per string.

The behaviour of the circuit is described by a first order differential equation, in which the unknown quantity is the voltage across the capacitor $v(t)$:

$$\frac{dv(t)}{dt} + \frac{v(t)}{R_{eq} \cdot C} = \frac{N_s \cdot V_{oc}}{R_{eq} \cdot C} \qquad (4)$$

The voltage signal must be continuous at time $t = t_0$, so the initial voltage $v(t=t_0)$ is the same voltage measured at the end of the previous transient.

$$v(t = t_0) = V_0 = \frac{I_{sc} \cdot N_p \cdot t_0}{C} \tag{5}$$

Therefore, the evolution of the voltage across the capacitor is defined by the following expression, which is the solution of the differential equation (4), according to the boundary condition (5):

$$v(t) = V_{oc} \cdot N_s + \left(\frac{I_{sc} \cdot N_p \cdot t_0}{C} - V_{oc} \cdot N_s \right) \cdot e^{\frac{-(t-t_0)}{R_{eq}C}} \qquad \text{for} \quad t_0 < t < \infty \tag{6}$$

As well-known, the evolution of the current in the capacitor is:

$$i(t) = C \cdot \frac{dv(t)}{dt} = \left(\frac{V_{oc} \cdot N_s}{R_{eq}} - \frac{I_{sc} \cdot N_p \cdot t_0}{R_{eq} \cdot C} \right) \cdot e^{\frac{-(t-t_0)}{R_{eq}C}} \qquad \text{for} \quad t_0 < t < \infty \tag{7}$$

As in the case of the voltage, the current must also be continuous at $t = t_0$

$$i(t = t_0) = I_{sc} \cdot N_p \tag{8}$$

The expression that links the capacitance value C with the switching time t_0, i.e., the time which separates the two different transients, is the following:

$$C = \frac{I_{sc} \cdot N_p}{V_{oc} \cdot N_s - R_{eq} \cdot I_{sc} \cdot N_p} \cdot t_0 \tag{9}$$

The final time t_f, which elapses between the closing of the circuit and the full charging of the capacitor, is the sum of the durations of the two transients. After the switching time t_0, the PV generator is assumed as a real voltage source and the behaviour of the circuit is defined by a differential equation of the first order with a time constant $\tau = R_{eq}C$. Thus, the final time t_f is:

$$t_f = t_0 + 5R_{eq}C \tag{10}$$

Fig. 7 shows the actual and simulated waveforms of current, voltage and power during the charging of a capacitor by a commercial PV module. The signals are different, especially around the maximum power point, due to the limitations of the simplified model here adopted. The exponential voltage signal, in the second part of the transient, appears constant since the starting voltage is near the final

voltage.

Combining (9) and (10), it is possible to obtain (11) which links the size of the capacitor to the duration throughout the transient:

$$C = \frac{t_f \cdot I_{sc} \cdot N_p}{V_{oc} \cdot N_s + 4 \cdot R_{eq} \cdot I_{sc} \cdot N_p} \qquad (11)$$

This expression depends on the main parameters of the PV generator: V_{oc}, I_{sc} of the PV module, the scale factors N_p, N_s and the generator equivalent resistance R_{eq}. The voltage and current parameters can be obtained from the manufacturer datasheet and N_p, N_s are a result of the design procedure.

The main drawback is that the generator equivalent resistance R_{eq} is not known a priori. For this reason, an approximate calculation of this parameter is proposed. The calculation of the values of the series and parallel resistances, in the single-diode model of solar cells, usually requires the solution of a non-linear system of equations. Other approaches [18] allow a direct calculation of these two values, avoiding the solution of difficult non-linear equations.

In order to size the capacitor, an accurate evaluation of the value of the equivalent resistance is not necessary. Then, as a first approximation, this value can be calculated assuming a straight-line passing between a fictitious point ($I_{sc};V_{mpp}$) and the point at open circuit conditions. Therefore, the approximate value of the equivalent resistance of the entire PV generator is a function of voltages V_{oc} and V_{mpp}, current I_{sc}, and scale factors N_p, N_s.

$$R_{eq} = \frac{V_{oc} - V_{mpp}}{I_{sc}} \cdot \frac{N_s}{N_p} \qquad (12)$$

The substitution of (12) in (11) yields an expression that links the size of the external capacitor to the duration of the transient, without the calculation of the equivalent resistance and that depends only on datasheet parameters and architecture of the PV generator:

$$C = \frac{t_f \cdot I_{sc} \cdot N_p}{V_{oc} \cdot N_s + 4 \cdot \dfrac{V_{oc} - V_{mpp}}{I_{sc}} \cdot \dfrac{N_s}{N_p} \cdot I_{sc} \cdot N_p} \qquad (13)$$

   III- Approximated formula for capacitive load

Near *STC* conditions, the voltage V_{mpp} of traditional crystalline silicon PV modules is about 80% of V_{oc}. Thus, a simpler expression of the equivalent resistance is:

$$R_{eq} \cong \frac{V_{oc} - 0.8 \cdot V_{oc}}{I_{sc}} \cdot \frac{N_s}{N_p} = 0.2 \cdot \frac{V_{oc} \cdot N_s}{I_{sc} \cdot N_p} \tag{14}$$

Substituting (14) in (13), the final expression for the capacitive load is:

$$C = A \cdot t_f \cdot \frac{I_{sc} \cdot N_p}{V_{oc} \cdot N_s} \cong 0.55 \cdot t_f \cdot \frac{I_{sc} \cdot N_p}{V_{oc} \cdot N_s} \tag{15}$$

The link between the total measurement time t_f and the size of the capacitor C is defined. The equation, solved in terms of the time, gives essentially the finding presented in [19]. The dimensionless coefficient A takes into account the approximations made to simplify the calculations. For this reason, theoretical calculations were compared with actual data, to check the value of A.

IV- Experimental results on actual PV arrays

The automatic data acquisition system, used to carried out measurements of array *I-V* curves, simultaneously detects voltage, current, irradiance and temperature. It is periodically calibrated and is made up of the following components:

- notebook PC;

- multifunction data acquisition device, equipped with one A/D converter (successive approximation, 16 bit-resolution, sampling rate up to 1.25 MSa/s) and multiplexer;

- differential probes for voltage measurements up to 1000 Vpk;

- current probes (Hall effect), for DC/AC measurements, peak values of 200-2000 Apk;

- secondary standard pyranometer and irradiance sensors based on mono and poly-crystalline silicon cells;

- thermometer (thermistor) for ambient temperature.

The measurement uncertainties are clarified below:

➢ for the irradiance G the absolute uncertainty is ± 20 W/m^2, for the ambient temperature T_a the absolute uncertainty is ± 0.2 °C, for the cell temperature T_C the absolute uncertainty is ± 2 °C;

- for the short circuit current I_{sc} and the open-circuit voltage V_{oc} of the PV generator, the corresponding relative uncertainties are $\pm 1\%$ and $\pm 0.1\%$;

- for the fill factor *FF*, defined as the ratio of the maximum power P_{mpp} to the product $V_{oc}{\cdot}I_{sc}$, the uncertainty is $\pm 2\%$);

- for the maximum power at standard test conditions $P_{mpp} = V_{mpp}{\cdot}I_{mpp}$ (*STC*), the measurement uncertainty is $\pm 4\%$).

The measurements were carried out to determine the parameters of the PV generators in conditions of natural sunlight and subsequently to return them at *STC* conditions. For each measurement, data of the modules, architecture of the PV generator and size of the capacitor are known. The total measurement time is long enough to allow to analyze all the operating points of the PV generator. Therefore all data in (15) are available, in this way it is possible to check the accuracy of the proportionality factor *A*.

The parameter *A* is calculated with data from more than 50 actual PV systems with different technologies and power ratings, distributed between 1 and 250 kW$_p$. The measured values (Table III) confirm the theoretical calculations: the mean value is 0.52 and the standard deviation is 0.03.

V- Capacitance sizing

It is very easy using (15) to size the capacitance for the designers of the *I-V* curve tracer and the *MPP* trackers. In particular, the parameters which play a role are the duration of the measurement and the characteristics of the PV generator.

In general, the *I-V* measurements or the scanning for *MPPT* must be carried out at constant ambient conditions (irradiance and temperature): according to [20], the maximum duration for the charging transient is 100 ms.

However, to trace the *I-V* curve with sufficient accurate points, it is recommended to choose capacitances so that the total test time is >20 ms. As previously discussed, the parasitic parameters generate swings during the first part of transient and the corresponding points (around I_{sc}) are not useful for tracing the *I-V* curve (they are omitted). Hence, for the conventional crystalline silicon

technologies, the external capacitance can be reduced to a few tens of microfarads, provided that a sufficiently accurate value of the short circuit current is not lost. Concerning Fig. 4, a good approximation of I_{sc} is achieved after the damping of swings occurring at 0.1 ms corresponding to a generator voltage of 3 V (a few percent of V_{oc}).

Known the range of acceptable durations, the range of capacitances to test real systems can be defined. Considering the 100-ms limit, it is possible to draw the graph in Fig. 8. This graph helps to find the maximum capacitance as a function of large voltage and current levels. The dashed hyperbolas show the array power calculated as $P_{array} = 0.7 \cdot V_{oc} \cdot I_{sc}$ with a typical value of fill factor ($FF=0.7$). For example, a PV system, consisting of $N_p=50$ parallel strings made of $N_s=16$ modules in series, must be tested to determine the output power. The parameters specified by the manufacturer at *STC* are: $I_{sc}=419$ A and $V_{oc}=602$ V (single module: $V_{oc}=37.6$ V, $I_{sc}= 8.38$ A). In this case during the test, if current and voltage of the system are those indicated by the manufacturer (*STC*), the capacitance is $C=35$ mF, corresponding to a duration $t_f =100$ ms.

On the other hand, the graph in Fig. 9 shows the capacitances that permit to test different PV systems in a shorter time (20 ms). In the example under consideration, the capacitance is $C=7$ mF. Therefore, a capacitance should be used in the range 7—35 mF, to obtain a duration between 0.02 to 0.1 s.

Real test conditions are different from *STC*: the measurements can be carried out at 600—1000 W/m^2 and thus the short circuit current may be considerably lower. In the same way, the cell temperature is a function of some parameters (ambient and installation conditions) and the open circuit voltage can change widely.

Designers of PV systems choose the number of modules to comply with both the maximum insulation voltage (1000 V) and the voltage range accepted by *MPPTs*, which is generally below 800 V. Thus, the number of modules that make up a string is in the range $N_s=10$—20. Even the maximum current generated by an array has a limit and the PV arrays have approximately a maximum number of strings in parallel $N_p=90$.

Fig. 10 shows the restricted area to be considered for the capacitance sizing to test large traditional

PV systems in 100 ms. For example, using a capacitor of 10 mF, a correct measurement of the *I-V* characteristic is possible with parameters of voltage and current above the dashed line.

Moreover, an analysis of the correct sizing of a capacitance to test single modules is done taking in account voltage V_{oc} and current I_{sc} of 20 different PV modules with a power between 220 and 250 Wp. All modules are made of crystalline silicon with the exception of one in amorphous silicon (a-Si). The modules are divided into two groups: in the first group there are modules with 96 cells (125 mm side) and they have $I_{sc} \approx 5$ A and $V_{oc} \approx 60$ V. In this case the optimum capacitance to measure the *I-V* curve in 100 ms should be ≈ 5 mF.

The second group of modules has $I_{sc} > 8$ A and $V_{oc} < 40$ V (60 cells, 156 mm side). The capacitor should have a capacitance of 10 mF. Only the a-Si module has different datasheet (62 Wp) and the required capacitance is ≈ 4 mF.

Therefore, the discussion about the capacitance can be summarized according to the type of Power Conditioning Unit (*PCU*) which manages the interface between the DC side and the AC side of the PV system. If a centralized *PCU* configuration, with high voltage and current levels of PV array, is examined, the optimum capacitance is within few tens of millifarads. If a string inverter is considered, the optimum capacitance is found in the range of few hundreds of microfarads. Finally, if the case of module integrated inverter (AC module) occurs, some millifarads represent the appropriate size of the capacitance. The durations of the presented *I-V* curve tracer are suitable for automatic data acquisition systems in which their sampling rates are within 10—50 kSa/s.

4.   Proposed MPPT technique

Due to the intrinsic characteristics of capacitor, its resistance changes from zero to infinity during charging. This property of capacitor is utilized for obtaining the *P-V* curve of a PV array. The charging time of the external capacitor is given by (15). Ref. [21] has proposed capacitor-based *MPPT*, but has failed to address some of the issues pertaining to the practical implementation of the *MPPT* algorithm.

The amount of C in (15) is chosen for the values of I_{sc} corresponding to low irradiance conditions, around 200 W/m^2 and a duration of a few milliseconds. However, in the event of uniform and full irradiance there is a substantial increase in the value of I_{sc} and the capacitor will be charged very quickly. In that event the measurement speed of *MPPT* system becomes important. This issue is addressed in this paper by using a fast scanning circuit.

In Fig. 11 the block diagram of the proposed MPPT is shown. Switch S1 is used to separate the DC-DC converter (with a supercapacitor for continuous power flow) from the PV array if the scanning of its *P-V* curve is carried out. Switch S2 is used to connect the scanning circuit to the PV array. Fig. 12 shows the connection diagram of the scanning circuit. When the *P-V* characteristic is scanned, S2 is closed and S1 is opened. Current through the charging capacitor is measured by a Hall-effect sensor. R1 and R2 are used for voltage division of the capacitor charging voltage during scanning. These resistors have large values so that they draw a negligible current during the charging of capacitor. A relatively small resistor is used to discharge the capacitor after the scanning is completed. The capacitor's charging voltage and current are multiplied by analog multiplier and its output is fed to a peak detector. When peak value at output of the multiplier is detected, the peak detector triggers the Sample and Hold (*S&H*) circuit into sample mode for 5μs and the corresponding voltage is held [22]. Low frequency pulse generator described in [23] is responsible for controlling the duration of the PV array scanning and the time interval between two successive scannings.

A short acquisition time of *S&H* is very important for determining accurate value of *MPP* voltage during uniform and full irradiance conditions. Also, the duration between two successive scannings of the array is long, typically 15—25 s as reported in [24], it is important to maintain a droopless operation during this period. For this purpose, an infinite *S&H* is utilized in the proposed circuit [25]. In the proposed circuit the voltage corresponding to *MPP* is first converted to digital form using an onchip analog to digital converter (*ADC*). This value is restored to analog form using digital to analog converter (*DAC*) on the same chip. This scheme has a number of advantages over traditional *S&H* which stores the held value on a hold capacitor. Firstly, because the stored value is recreated using a

DAC, the circuit does not suffer from any droop problems associated with storing voltages on a hold capacitor for relatively long periods of time. Secondly, both the purposes of short acquisition time and zero droop rate are achieved which is not possible through the use of a hold capacitor.

After scanning the *P-V* curve, voltage corresponding to *MPP* is held by *S&H* as V_{mpp}. The pulse width modulation circuit compares the array voltage with V_{mpp} and adjusts the duty cycle of DC-DC converter to operate the PV array at its *MPP* [26].

5.   Simulation results

The proposed circuit is simulated in Proteus software [27]. It is applied to a single PV module characterized by $P_{mpp}(STC)$ =50 Wp, V_{oc} =21.8 V, I_{sc} =3.14 A and equipped with bypass diodes. The shade from a partial transparent obstacle is simulated by a decrease of irradiance from G_{STC} down to 850 W/m^2. The value of the external capacitor was taken to be 300 µF, in order to recognize the *GM* within a few milliseconds. Figures 13, 14, and 15 show the following quantities during the simulation:

1. Output of the multiplier: this gives the value of the array's power during the scanning of its *P-V* curve. This value is monitored by the peak detector and it triggers the *S&H* in sampling mode when peak value of power is detected.

2. The output of the *S&H* which corresponds to V_{mpp} and it is utilized by the *PWM* controller as reference voltage.

3. Fraction of voltage across the charging capacitor during the scanning of the PV curve.

4. Signal at the control pin of *S&H*. As discussed previously, when the peak detector detects a peak at the output of the multiplier, this signal goes low which triggers the *S&H* into sampling mode to sample and hold the voltage corresponding to that peak.

Even though the acquisition time of the *S&H* is about 5µs, in the simulations a pulse of a larger duration at the control pin of *S&H* has been shown for clarity of the figures. As a result of it, the circuit will track a slightly higher value than the actual value of the *MPP* voltage during simulations.

Fig. 13 shows the acquisition of V_{mpp} in case of a single peak on the *P-V* curve, this corresponds to uniform irradiance conditions. As is evident from the figure, the circuit is able to track the unique peak on the *P-V* curve under uniform irradiance. The circuit in this case acts like a conventional *MPPT*. The same Fig. also shows the charging current of the external capacitor which has been referenced to the right Y-axis.

The performance of the proposed circuit during the presence of multiple peaks due to partial shading condition was checked. Fig. 14 shows the case in which two peaks are present on the *P-V* curve, i.e., at the output of the multiplier. As can be seen, the algorithm first tracks a local peak but when a global peak is encountered, voltage corresponding to that peak is sampled by S&H. The figure indicates that after tracking of a local peak, the circuit is not trapped at that point but tracks the global peak when it is observed later during the scanning. Fig. 15 shows the case when a global peak is tracked, the circuit ignores a local peak encountered subsequently during the scanning.

6. Conclusions

In the first part of this paper, the transient charging of a capacitor supplied by a PV generator is analysed in depth, to size the proper *I-V* curve tracers. The swings in the current signal, due to parasitic capacitance and inductance of the PV generator, cause the loss of the initial portion of the transient evolution and thus the amplitude and duration of swings must be minimised. This permit a correct estimation of short circuit current. A simple formula links the capacitance and the total duration through the short circuit current, the open circuit voltage and their scale factors. Theoretical

calculations are compared with measurements, to check the accuracy of the model adopted. The capacitance ranges are determined according to the configuration of the power conditioning units (centralised units, string inverters and AC modules).

In the second part a maximum power point tracker for photovoltaic arrays under partial shading condition is proposed. The *P-V* curve of a photovoltaic array has multiple peaks among which there is one global peak. Periodic scan sequence of a PV array during partial shading condition is employed for tracking of *GMPP*. The duration of such a scan is long and it results in power loss. The proposed *MPPT* circuit aims to reduce the time duration required for scanning the *P-V* curve of the array. The circuit is also easy to implement as it does not require complex computation. Simulations of the circuit are performed using Proteus software. The circuit is able to track the *MPP* of the array under uniform as well as under partial shading conditions.

References

[1] Filippo Spertino, Paolo Di Leo, Valeria Cocina, Which are the constraints to the photovoltaic grid-parity in the main European markets?, *Solar Energy*, vol. 105, 2014, pp. 390-400, http://dx.doi.org/10.1016/j.solener.2014.03.021.

[2] Grid connected photovoltaic systems-minimum requirements for system documentation, commissioning test and inspection, *IEC Standard 62446*, 1st edition 2009.

[3] J.V. Muñoz, G. Nofuentes, J. Aguilera, M. Fuentes, P.G. Vidal, "Procedure to carry out quality checks in photovoltaic grid-connected systems: Six cases of study," *Applied Energy*, vol. 88, 2011, pp. 2863-2870.

[4] Nuri Gokmen, Engin Karatepe, Faruk Ugranli, Santiago Silvestre, Voltage band based global MPPT controller for photovoltaic systems, *Solar Energy*, vol. 98, 2013, pp. 322-334, http://dx.doi.org/10.1016/j.solener.2013.09.025.

[5] E. Koutroulis, "A new technique for tracking the global maximum power point of PV arrays under partial shading conditions," *IEEE Journal of Photovoltaics*, vol. 2, 2012, pp. 184-190.

[6] Mohammad H. Moradi, S.M. Reza Tousi, Milad Nemati, N. Saadat Basir, N. Shalavi, A robust hybrid method for maximum power point tracking in photovoltaic systems, *Solar Energy*, vol. 94, 2013, pp. 266-276, http://dx.doi.org/10.1016/j.solener.2013.05.016.

[7] Mohammad H. Moradi, Ali Reza Reisi, A hybrid maximum power point tracking method for photovoltaic systems, *Solar Energy*, vol. 85, 2011, pp. 2965-2976, http://dx.doi.org/10.1016/j.solener.2011.08.036.

[8] G. Petrone, G. Spagnuolo, R. Teodorescu, M. Vitelli, "Reliability issues in photovoltaic power processing systems", *IEEE Transactions on Industrial Electronics*, vol. 55, 2008, pp. 2569-2580.

[9] Mutlu Boztepe, Francese Guinjoan, Guillermo Velasco-Quesada, Santiago Silvestre, Aissa Chouder, and Engin Karatepe, "Global MPPT scheme for photovoltaic string inverter based on restricted voltage window search algorithm," *IEEE Transactions on Industrial Electronics*, vol. 61, 2014, pp. 3302-3312.

[10] Aymen Chaouachi, Rashad M. Kamel, Ken Nagasaka, A novel multi-model neuro-fuzzy-based MPPT for three-phase grid-connected photovoltaic system, *Solar Energy*, vol. 84, 2010, pp. 2219-2229, http://dx.doi.org/10.1016/j.solener.2010.08.004.

[11] A. Murtaza, M. Chiaberge, F. Spertino, D. Boero, M. De Giuseppe, "A maximum power point tracking technique based on bypass diode mechanism for PV arrays under partial shading," *Energy and Buildings*, vol. 73, pp. 13-25, 2014.

[12] H. Patel, V. Agarwal, "Maximum power point tracking scheme for PV systems operating under partially shaded conditions," *IEEE Transactions on Industrial Electronics*, vol. 55, 2008, pp. 1689-1698.

[13] Kai Chen, Shulin Tian, Yuhua Cheng, Libing Bai, "An improved MPPT controller for photovoltaic system under partial shading conditions," *IEEE Transactions on Sustainable Energy*, vol. 5, 2014, pp. 978-985.

[14] M.E. Glavin, W.G. Hurley, Optimisation of a photovoltaic battery ultracapacitor hybrid energy storage system, *Solar Energy*, vol. 86, 2012, pp. 3009-3020, http://dx.doi.org/10.1016/j.solener.2012.07.005.

[15] F. Spertino, A. Ciocia, F. Corona, P. Di Leo, F. Papandrea, An Experimental Procedure to Check the Performance Degradation On-Site in Grid-Connected Photovoltaic Systems, 40th IEEE Photovoltaic Specialists Conference, Denver, Colorado, July 2014, pp. 2600-2604.

[16] F. Spertino, J. Sumaili, H. Andrei, G. Chicco, "PV module parameter characterization from the transient charge of an external capacitor," *IEEE Journal of Photovoltaics*, vol. 3, 2013, pp. 1325-33.

[17] *Standard IEC 60891:2009-12 Photovoltaic devices - Procedures for temperature and irradiance corrections to measured I-V characteristics.*

[18] J.Accarino, G. Petrone, C.A. Ramos-Paja, G. Spagnuolo, "Symbolic Algebra for the Calculation of the Series and Parallel Resistances in PV module model", 4th International Conference on Clean Electrical Power: Renewable Energy Resources Impact, ICCEP, pp. 62-66, 2013.

[19] M. M. Mahmoud, "Transient analysis of a PV power generator charging a capacitor for measurement of the I-V characteristics," *Renewable Energy*, vol. 31, 2006, pp. 2198-2206.

[20] *Commission of the European Communities, Joint Research Centre, "Guidelines for the Assessment of Photovoltaic Plants – Initial and Periodic Tests on PV Plants, Document C", European Commission Joint Research Centre, Ispra, Italy, 1995*.

[21] K. S. Parlak, Hayrettin Can, "A new MPPT Method for PV array under partially shaded conditions," 3rd IEEE Symposium on Power Electronics for Distributed Generation Systems, pp. 437-441, 2012.

[22] Yingying Kuai, S. Yuvarajan, "An electronic load for testing photovoltaic panels," *Journal of Power Sources*, vol. 154, 2006, pp. 308-13.

[23] Linear Technology LTC6991, Resettable Low Frequency Oscillator, datasheet available at: http://www.linear.com/product/LTC6991.

[24] B. Bekker, H. J., Beukes, "Finding an optimal PV panel maximum power point tracking method," IEEE, 7th AFRICON Conference, 2004, vol. 2, pp. 1125-1129.

[25] Mike Byrne, "Implement infinite sample and hold circuits using analog input/output ports," Analog Devices Application Note AN-284.

[26] J. Ahmad, "A fractional open circuit voltage based maximum power point tracker for photovoltaic arrays," 2nd IEEE International Conference on Software Technology and Engineering, vol. 1, 2010, pp. 247-251.

[27] Cui Yan, Yao Wen, Luo Jinzhao, Bai Jingjing, "PROTEUS-based simulation platform to study thephotovoltaic cell model under partially shaded conditions," Electric Information and Control Engineering (ICEICE), 2011 International Conference on, pp. 3446 – 3449.
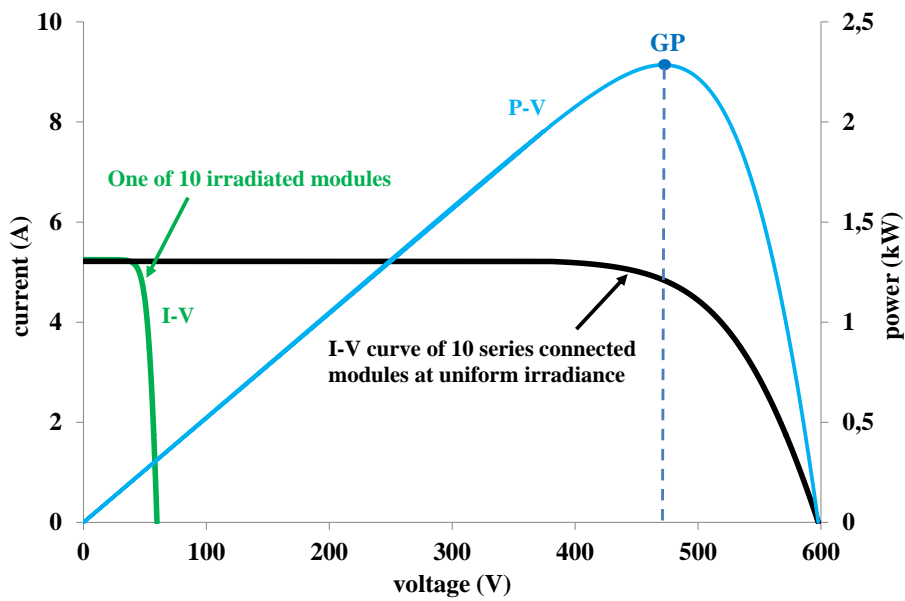
Fig. 1 *I-V* and *P-V* characteristics of a PV string made of ten series modules under uniform irradiance.

E

r
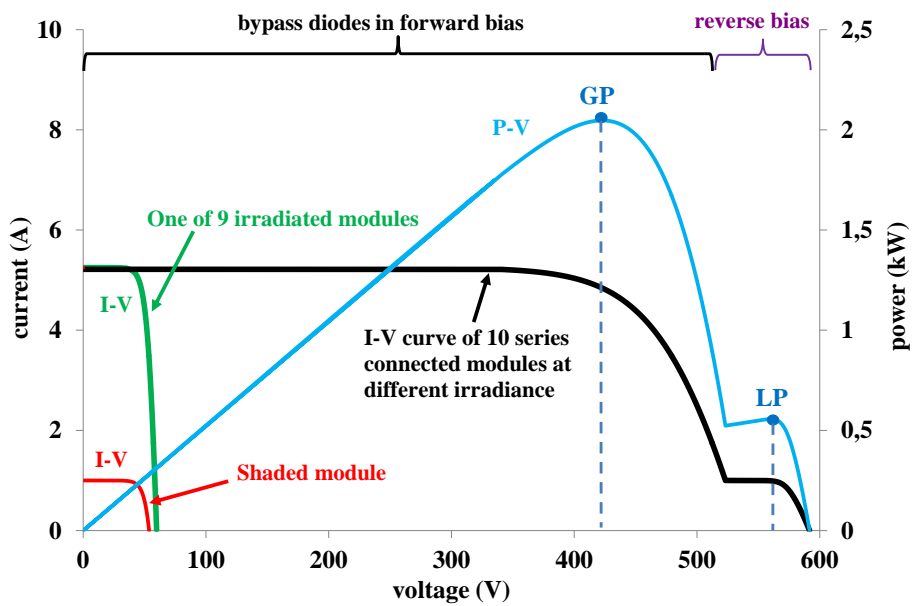
Fig. 2 *I-V* and *P-V* characteristics of a PV string made of ten series modules under partial shading conditions.
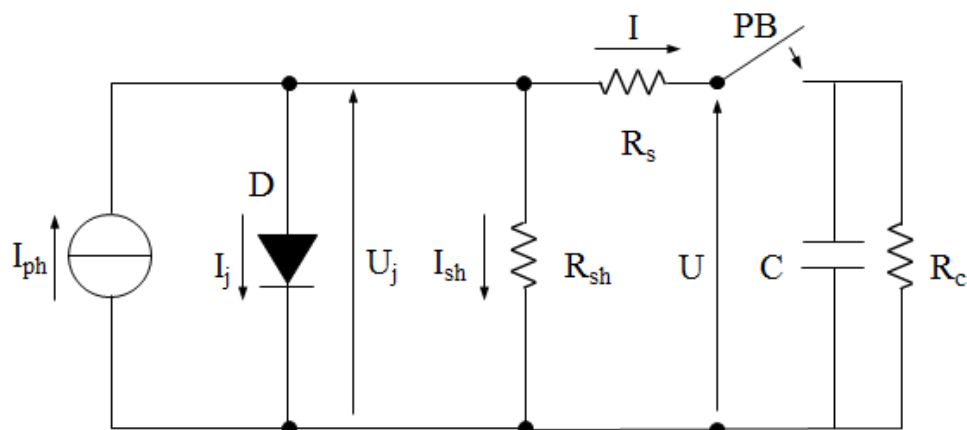
Fig. 3: Equivalent circuit of a solar cell which supplies an external capacitor by a power breaker.
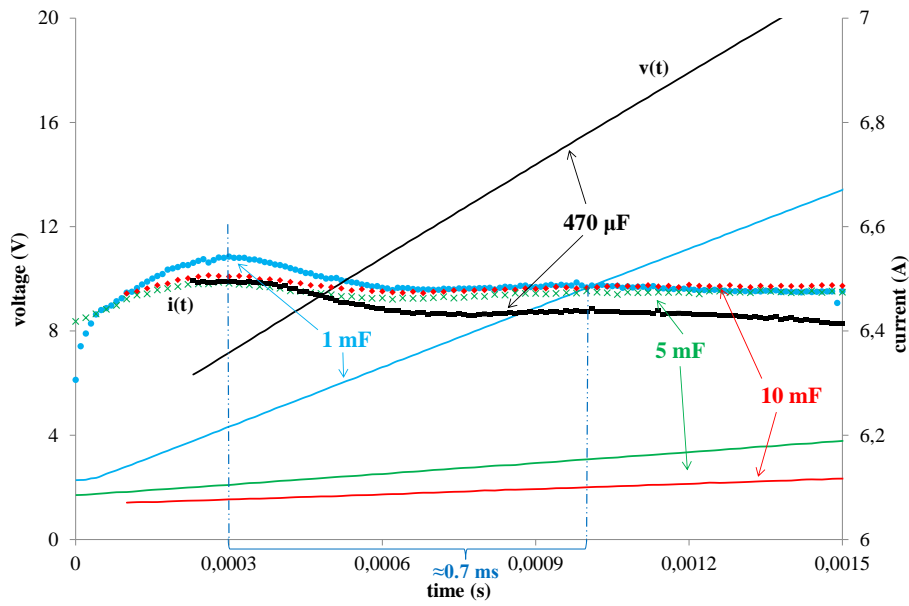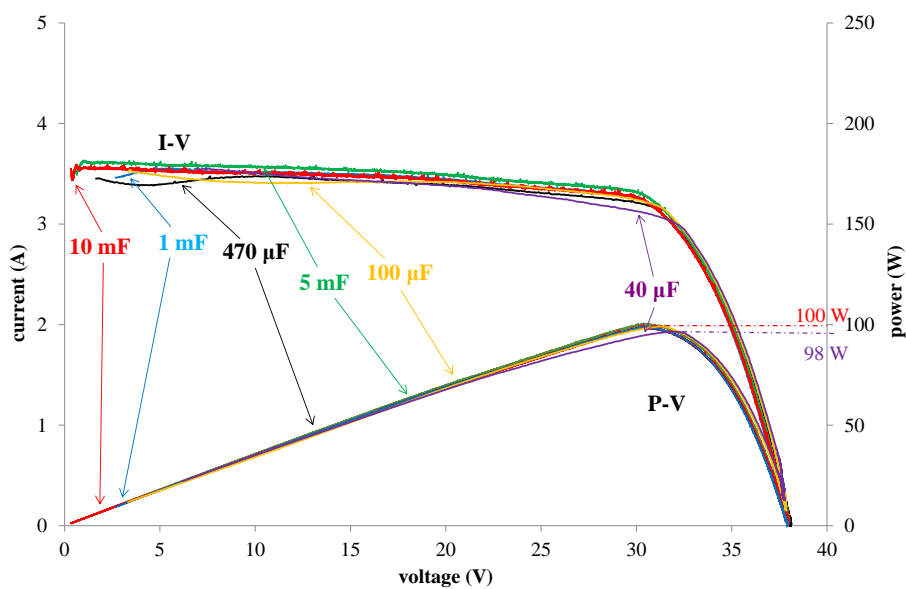

a)
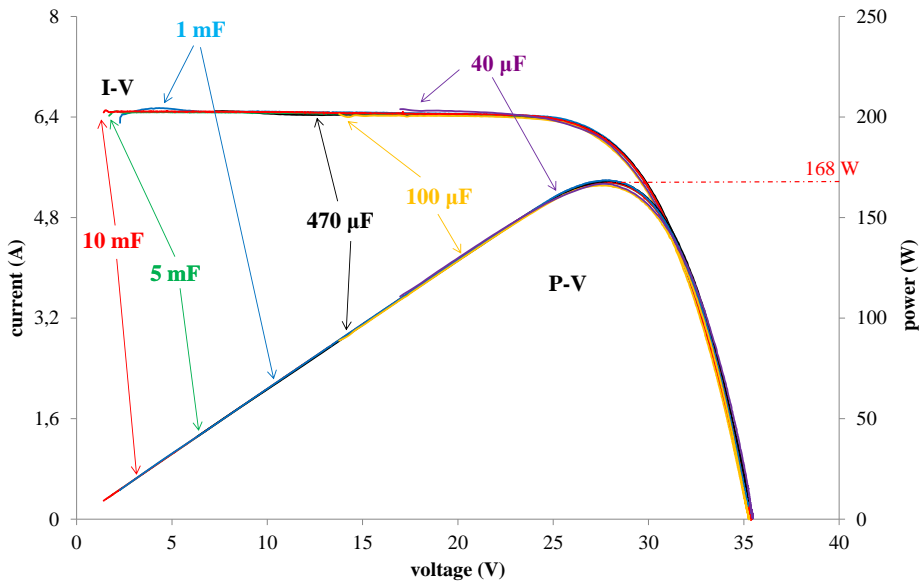
b)

Fig. 4 Current and voltage signals during the transient charging of different capacitors supplied by a p-Si module and *I-V*/*P-V* curves.
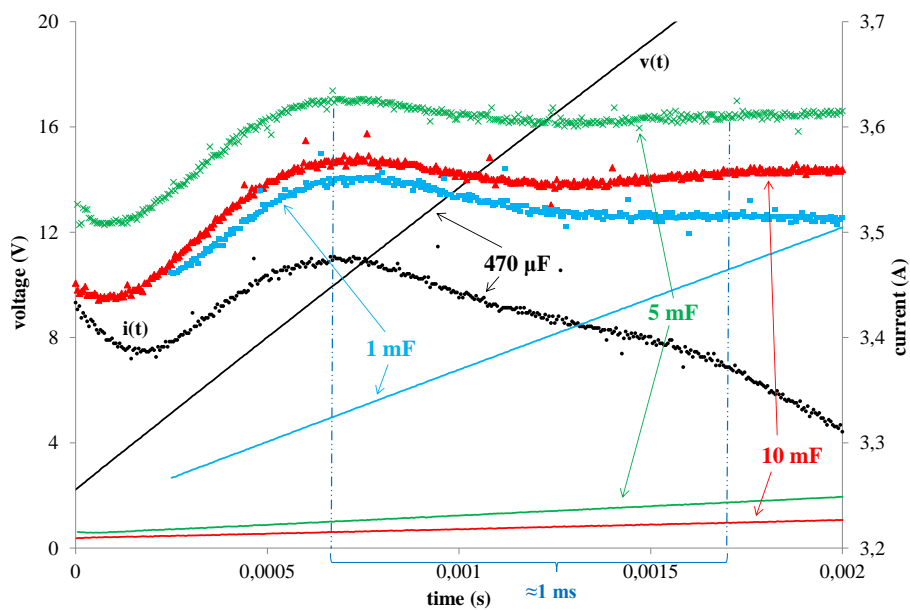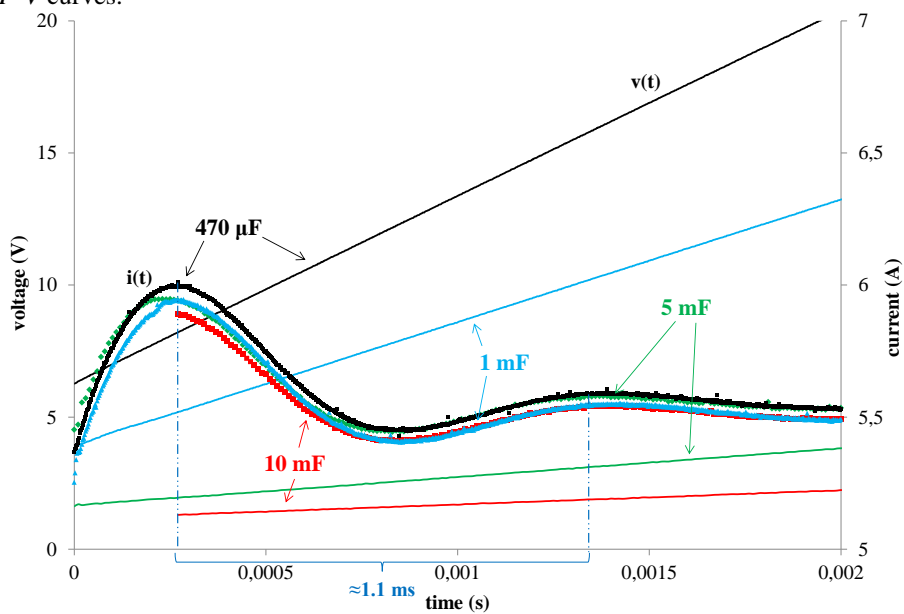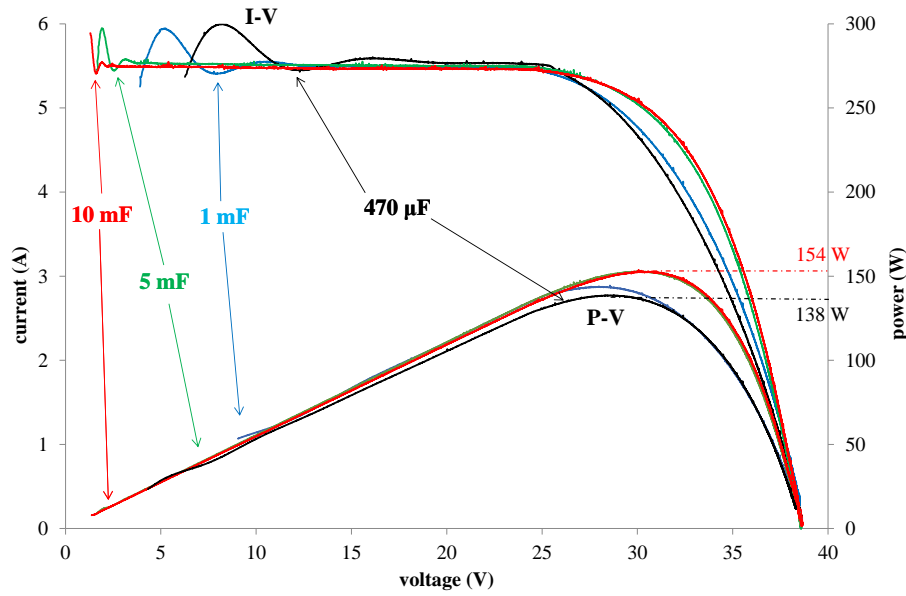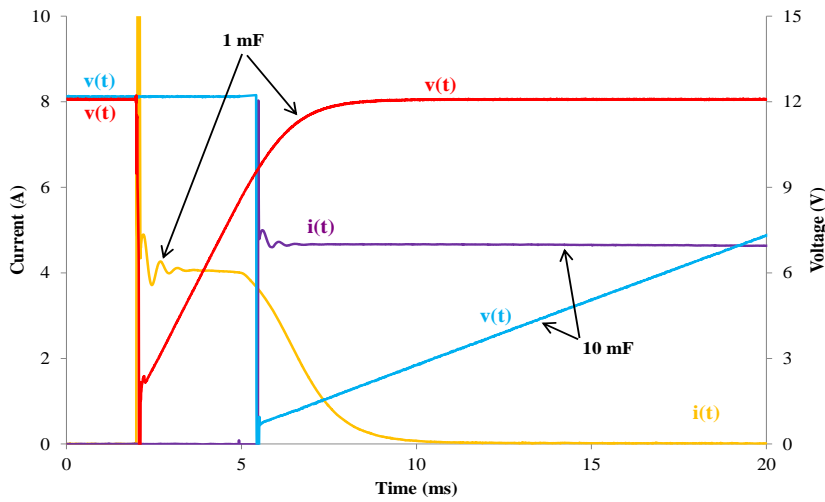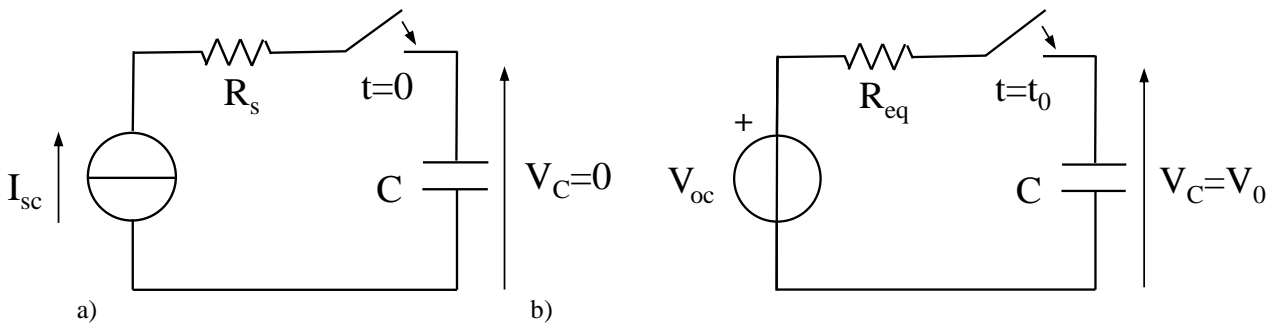
Fig. 5 Current and voltage signals during the transient charging of different capacitors supplied by a m-Si module and *I-V*/*P-V* curves.

b)

Fig. 6 Current and voltage signals during the transient charging of different capacitors supplied by a hetero-junction *m-Si/a-Si* module and *I-V/P-V* curves.

Fig. 7 Current and voltage signals during the transient charging of different capacitors supplied by a *BSC* module.

Fig. 8 a) Equivalent circuit valid for the first interval of the capacitor charging; 6.b) Equivalent circuit valid for the successive interval of the capacitor charging.
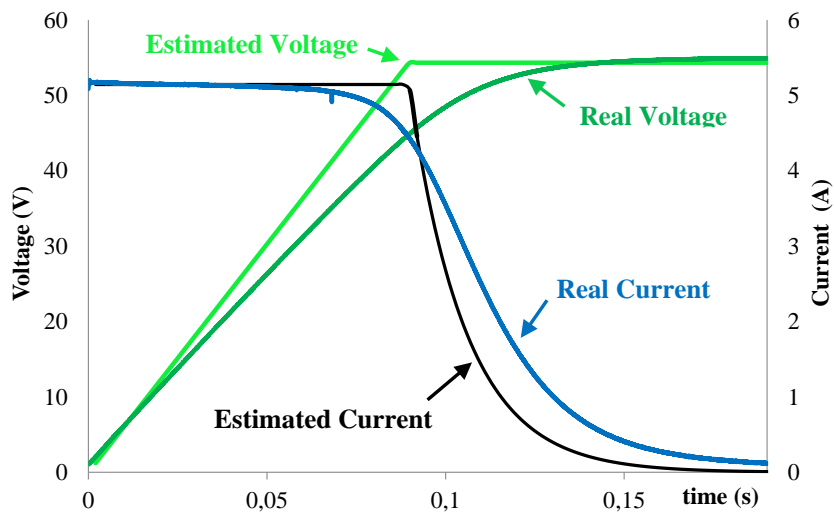
Fig. 9 Measured vs. simulated current and voltage signals during the capacitor charging by a *p-Si* module.
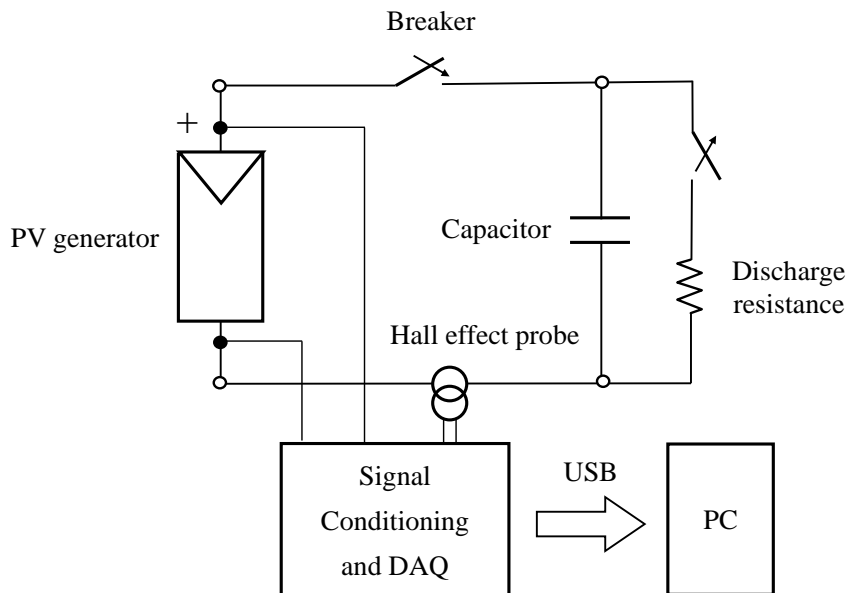
Fig. 10 Scheme of the measuring circuit of PV generators by capacitor charging method
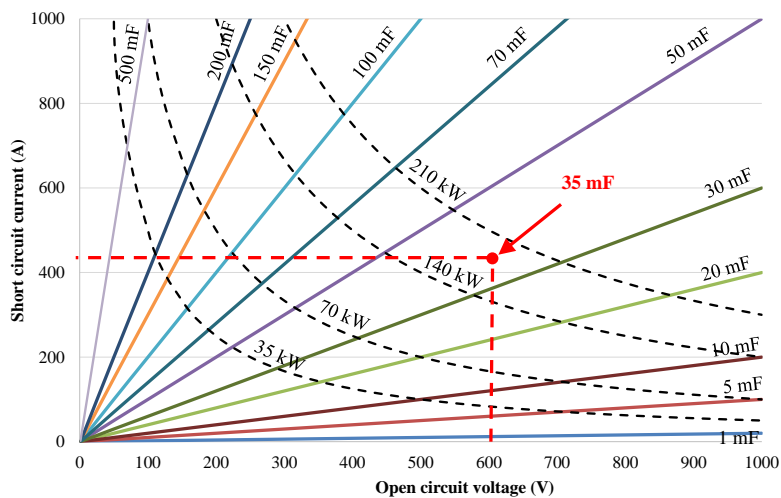
Fig. 11 Capacitance sizing to keep the test duration = 0.1 s, as a function of V_{oc} and I_{sc} of the PV array.
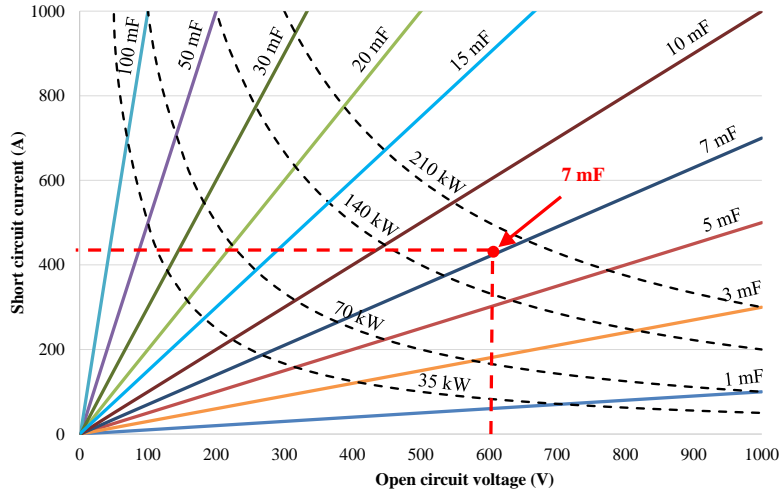
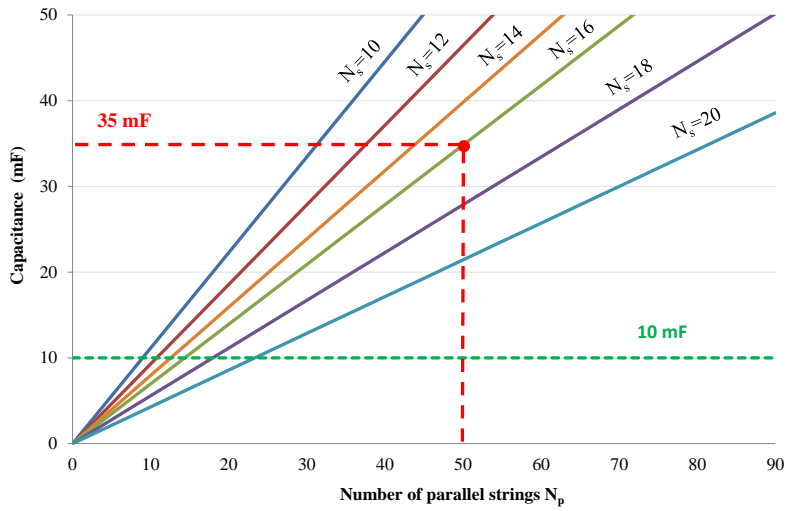Fig. 12 Capacitance sizing to keep the test duration = 0.02 s, as a function of V_{oc} and I_{sc} of the PV array.

Fig. 13 Capacitance sizing to keep the test duration = 0.1 s, as a function of the number of parallel strings N_p and the number of series modules N_s of commercial PV arrays (V_{oc} = 37.6 V, I_{sc} = 8.38 A for a single module).
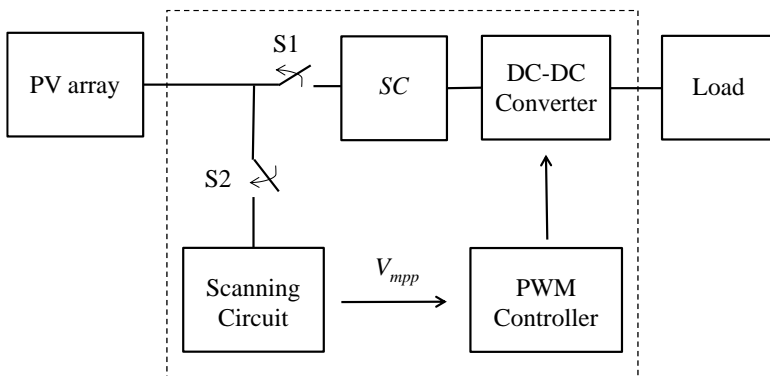

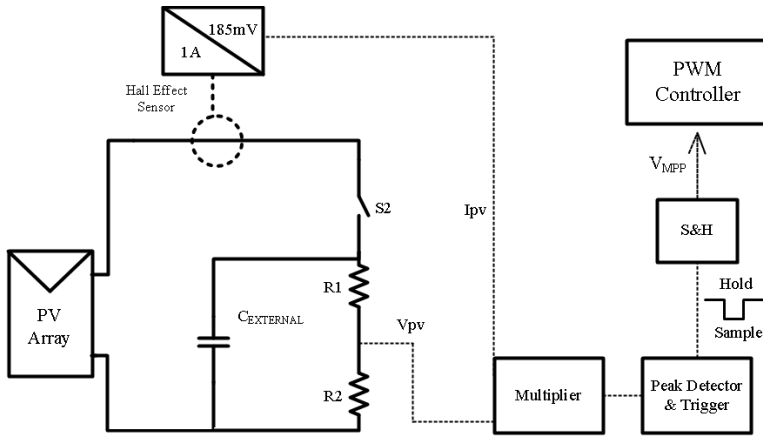Fig. 14 Block diagram of the proposed MPPT technique.
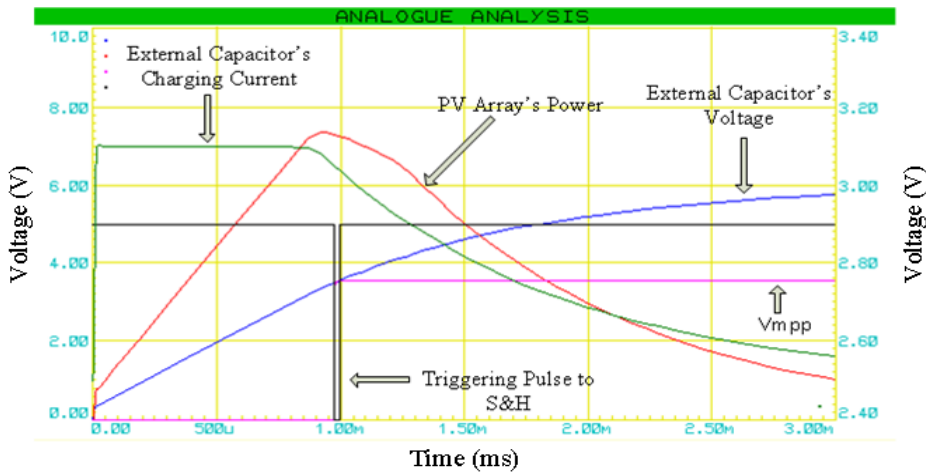
Fig. 15 Circuit diagram of the scanning circuit.

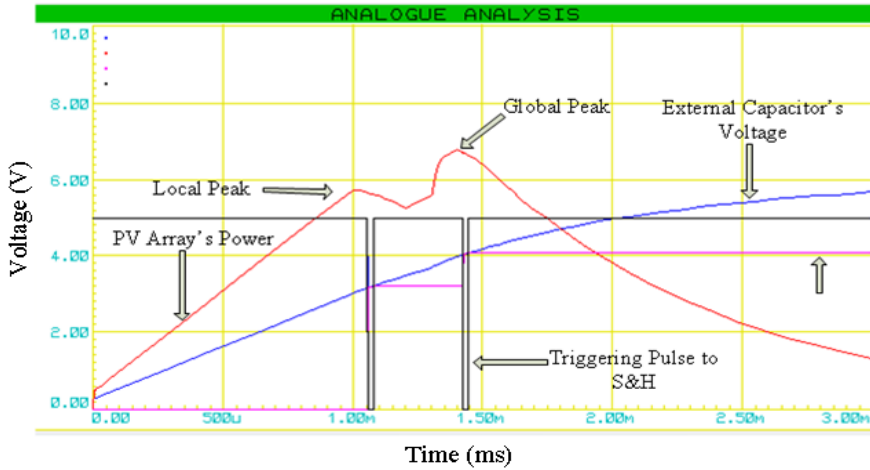Fig. 16 Acquisition of V_{mpp} in case of a single maximum.

Fig. 17 Acquisition of V_{Ref} in case of multiple maxima, first a local maximum is tracked but, when a global maximum is encountered, voltage corresponding to that maximum is sampled and held.
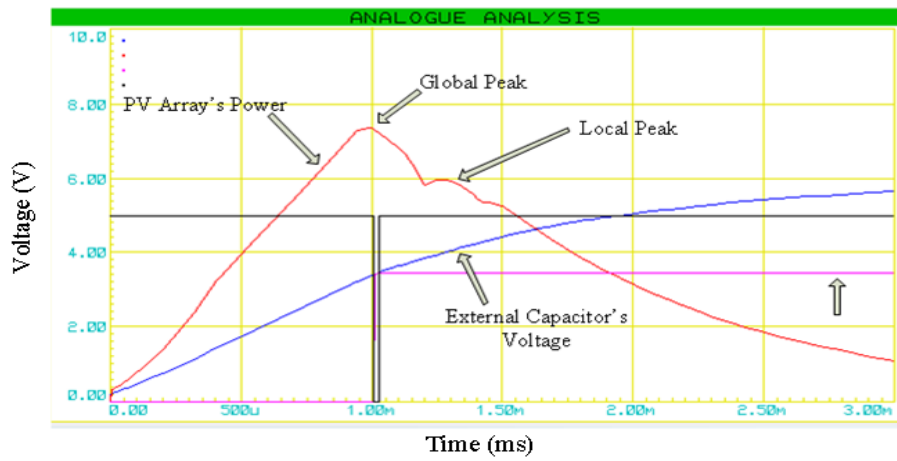
Fig. 18 Acquisition of V_{Ref} in case of two maxima, after the identification of GMPP any subsequent local maximum is ignored.

Table I. Main parameters of the capacitor charging method applied to a conventional PV module

C (μF)	t_f (ms)	P_{mpp} (W)	V_{mpp} (V)	I_{mpp} (A)
20000	211.4	163	27.9	5.9
10000	126.0	166	27.7	6.0
5000	44.8	165	27.8	5.9
1000	10.2	163	28.0	5.8
500	5.0	165	27.7	5.9
240	2.2	164	27.7	5.9
100	1.1	165	27.8	6.0
40	0.5	164	27.6	5.9

Table II. Parameters of the capacitor charging method applied to an unconventional PV module

C (μF)	t_f (ms)	P_{mpp}(STC)	V_{mpp}(STC)	I_{mpp}(STC)
10000	37.2	41.9 W	9.8 V	4.3 A
1000	7.3	35.2 W	9.3 V	3.8 A

Table III. .Experimental verification of proportionality factor *A (short list)*

P_{mpp} (kW)	Tech.	A
228,2	p-Si	0,55
189,0	p-Si	0,53
172,3	p-Si	0,54
170,5	m-Si	0,55
169,0	m-Si	0,54
168,7	p-Si	0,52
94,70	m-Si	0,53
92,80	m-Si	0,54
86,50	m-Si	0,55
81,70	m-Si	0,56
71,26	m-Si	0,55
56,10	m-Si	0,53
51,05	p-Si	0,52
48,08	p-Si	0,52
3,527	m-Si	0,52
3,512	m-Si	0,52
0,214	m-Si	0,52